buildings

MDPI

Article

Study on the Performance of a New Ultra-Low Temperature Air Source Heat Pump (ASHP) Unit in Cold Regions

Yanqiang Di [1,*], Chen Zhao [1], Xueli Lian [1], Xiaolong Li [1], Daorina Bao [2] and Jinxing Liu [3]

[1] China Academy of Building Research, Beijing 100013, China
[2] College of Energy and Power Engineering, Inner Mongolia University of Technology, Hohhot 010051, China
[3] Inner Mongolia Hengdong Group Huilong Coal Co., Ltd., Ordos 010308, China
* Correspondence: yanqiangdi@126.com

Abstract: Low air temperature and frosting have been reported as the critical factors that greatly attenuate the efficiency and performance of the ASHP in cold regions. In order to ensure the potential prevalence of the ASHP in cold regions of China, a new ultra-low temperature ASHP unit was developed, and the field measurement was carried out in an office building where these ASHP units were installed in Shanxi Province. Results showed that a coefficient of performance (*COP*) of 1.83 was obtained at the ultra-low environmental temperature of −25 °C. Meanwhile, measured results indicated significant frosting suppression and improved heating performance under three typical frosting conditions. In addition, long-term measurement results revealed that the mean *COP* and COP_{sys} reached up to 3.34 and 2.63, respectively, indicating a higher performance in the cold regions of China. Consequently, the corresponding CO_2 emission reached 11.3 kg per year and per square meter, and the annual total cost on the unit reduced by 15.8% compared with the conventional ASHP, which meant that the total investment could be covered in the second year. The reduced CO_2 emission and the annual cost implied that the ASHP unit could produce better environmental and economic benefits. Findings of this study revealed that this ultra-low temperature ASHP unit had a better performance under cold environment, which offered a possibility for the prevailing of the ASHP in cold or extremely cold regions, as well as could contribute to the carbon peaking and neutralization.

Keywords: ultra-low temperature; ASHP; cold regions; performance

check for updates

Citation: Di, Y.; Zhao, C.; Lian, X.; Li, X.; Bao, D.; Liu, J. Study on the Performance of a New Ultra-Low Temperature Air Source Heat Pump (ASHP) Unit in Cold Regions. *Buildings* **2023**, *13*, 2107. https://doi.org/10.3390/buildings13082107

Academic Editor: Vincenzo Costanzo

Received: 30 June 2023
Revised: 1 August 2023
Accepted: 15 August 2023
Published: 20 August 2023

1. Introduction

As an effective energy-conservation technology, the Air Source Heat Pump (ASHP) has been gaining more and more attention throughout the world in recent years, and it has also been included as a renewable energy solution by the European Union, Japan, and China [1,2]. The 'Clean Heating' policy of North China [3] has, since 2017, made the ASHP become an ideal option to get rid of coal. As a result, the ASHP has been regarded as a promising technology and is widely used in North China for heating.

The northwest of China is an extremely cold region; because of the large span between east and west, the climate of different regions is very different. According to the typical annual meteorological parameters in Northwest China, the lowest ambient temperature can reach −39 °C. Hence, the performance of the ASHP was inevitably compromised in the winter in Northwest China. The volumes of the refrigerant in the compressor expand due to the reduction of evaporative temperature and pressure, resulting the reduction of mass flow rate for the total refrigerant and the compromised heating capacity of the unit [4,5]. It is well known that the lower the ambient temperature at which ASHP operates stably, the better the low temperature performance. Wu et al. [6] studied the system *COP* which ranged from 1.63 to 2.17 for an outdoor temperature range of −24.7 to 15.0 °C. Safa et al. [7] investigated ASHP performance at the Archetype Sustainable Twin House, Ontario, Canada; the *COP* of the ASHP ranged from 1.79 to 5.0 for an outdoor temperatures of −19 °C to 9 °C. Zhang et al. [8] studied the application results of an ASHP in Harbin, the coldest area in China, the *COP*s ranged from 1.04 to 2.44 for the low temperatures of −20.9 °C to −10.4 °C. Zhang et al. [9] found the *COP* of ASHP varied from 1.8 to 4.2 as the outdoor air temperature increased from −18.4 °C to 6.9 °C. In addition, the minimum ambient temperature of ASHPs in relevant Chinese Standards GB/T 25127.1 [10] and GB/T 25127.2 [11] only reaches −20 °C, and the allowed *COP* cannot be lower than 1.8. It can be seen that the low temperature application ranges of ASHPs need to be further expanded, and the *COP* also needs to be further improved.

Moreover, the frosting would occur on the fin surface of the outdoor heat exchanger (the evaporator) of the ASHP unit in winter if the fin surface temperature of the outdoor heat exchanger was lower than the dew point temperature and the freezing temperature of the outdoor air [12–15]. Previous studies showed that the mean *COP* of the ASHP units would be reduced by 35–60%, leading to a 30–57% reduction in heating capacity [16–20]. Therefore, it is significant to improve the adaptability of the ASHP in cold and extremely cold climates, as well as enhance the frosting suppression capacity, in order to ensure the high performance of the ASHP.

Considering the attenuated performance of the ASHP in Northwest China, a new ultra-low ASHP unit was developed and installed in an office building in Shanxi Province in China. And the field measurements were conducted in this building to study the performance of the new ASHP unit under typical frosting condition and long-term operation. Additionally, the environmental and economic benefits of the ASHP were also analyzed. The relevant results would provide a strong possibility for the prevailing of the ASHP in cold and extremely cold regions.

2. Methods

2.1. Description of the Ultra-Low Temperature ASHP Unit

A new ultra-low temperature ASHP unit was invented and developed by the authors, which can provide a reliable solution for the adaptability of the ASHP to cold and extremely cold climates, as well as enhance the frosting suppression at low environmental temperature. The schematic diagram of the new ultra-low ASHP unit was shown in Figure 1. A special rotary compressor that could replenish the refrigerant vapor and increase the enthalpy during the operation was adopted in the new ASHP unit. In addition, the refrigerating circle, specifically the system including the compressor, condenser and evaporator, was also improved and optimized. The detailed parameters of the components are given in Table 1.

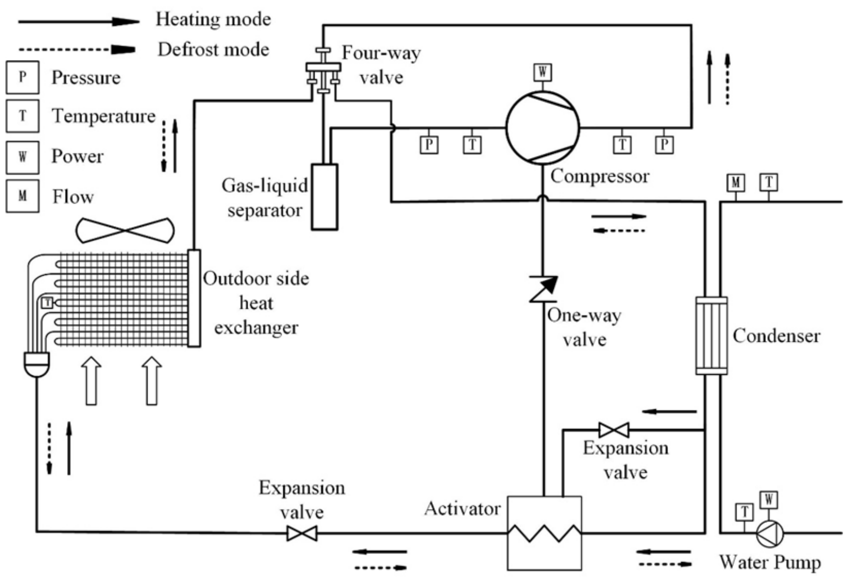

Figure 1. Schematic diagram of the new ultra-low ASHP unit.

Table 1. Components parameters of new ASHP unit.

Component	Project	Unit	Parameter
Compressor	Number	/	1
	Type	/	Rotary
	Rated speed	rps	70
	Volume	m^3/rev	4.24×10^{-5}
	Refrigerant	/	R410A
Outdoor heat exchanger (Evaporator)	Number	/	1
	Type of the fins	/	Hydrophilic corrugated wavy fins
	Dimensions	mm	1550 × 750 × 80
	Thickness of the fin	mm	0.1
	Distance between adjacent fins	mm	1.8
	Diameter of the tube	mm	7
	Distance between adjacent tubes	mm	25
	Row of the tubes	/	3
	Heat exchange area	m^2	65
Outdoor fan	Number	/	2
	Type	/	Brushless DC Motor
	Range of the air flow rate	m^3/s	0~2.5
	Rated air flow rate	m^3/s	2.5

The test was carried out in an experimental psychrometric chamber, where required test conditions can be provided and maintained. The sensors and transducers were connected to a computerized measuring system to monitor in real-time and record the operating parameters.

As shown in Table 2, the performance of the new ASHP unit was tested at the dry bulb temperature of −25 °C, which was 5 °C lower than the test requirements on the performance for ASHP unit that recommended by the Chinese Standards of GB/T 25127.1 and GB/T 25127.2. Hence, referring the condition of −20 °C for ASHPs in the Chinese Standards of GB/T 25127.1 and GB/T 25127.2, the supply hot water temperature of the new ASHP unit was set at 41 °C, and *COP* was not lower than 1.8. In addition, based on ASHP products on the market, the heating power of the new ASHP unit was set at 7 kW at −25 °C conditions. Results showed that a heating power of 7.5 kW and a *COP* of 1.83 were observed, which were 7% and 1.7% higher than the expected design values. The validation indicated that the new ultra-low ASHP unit had a better heating capacity and efficiency under cold conditions.

Table 2. Comparison between the designed and measured values of the new ASHP unit.

Critical Parameters	Designed Value	Measured Value
Dry bulb/Wet Bulb temperature (DB/WB) (°C)	−25/-	−25/-
Supply hot water temperature (°C)	41	41
Heating power(kW)	7	7.5
COP	>1.8	1.83

2.2. Field Measurement Protocols

In order to test the practical performance of this new ASHP unit, an office building in Shanxi Province was selected, located in the cold region of China. In total, 2 ASHP units were installed to provide heating service for this building. A 38-day field measurement was carried out during the heating season in 2022 in this building. A sophisticated monitoring system was also available in this building to provide real-time data of these ASHP units. The temperature and humidity data of the region where the building is located was −14.7 °C and 47% in winter, respectively. The annual heating season lasts 151 days in total. The heating area of this building was 650 m^2, and the radiant floor heating system was selected as the heating terminal.

The measuring system was established to acquire the critical data of the units, including the temperature and humidity sensors, the heating power sensors, and the electromagnetic flowmeter. These data were automatically recorded with a time interval of 60 s. For outdoor measurement, 1 recorder was installed near the outdoor heat exchanger to acquire the outdoor air temperature and relative humidity. The recorder had an accuracy of ±0.15 °C for temperature and ±3.5% for relative humidity. The measure ranges for the temperature and humidity were −20~70 °C and 0~100%, respectively. For indoor measurement, 1 recorder was installed in the testing room, with the same accuracies and ranges as those of the outdoor recorder.

For the measurement of ASHP units, 2 PT1000 sensors were installed in the suction pipe and discharge pipe of the compressor, respectively, to acquire the temperature data of the inlet and outlet of the compressor. In addition, 2 PT1000 temperature sensors were installed at the coil of the outdoor heat exchanger, one in the middle part and the other in the lower part of the coil, to monitor the temperature changes of the coils. These 4 PT1000 temperature sensors had an accuracy of ±0.15 °C and the range of −40~140 °C. Meanwhile, 2 pressure sensors were installed in the suction line and discharge line of the compressor to acquire the pressure changes of the compression during the whole field measurement. The accuracy of the pressure sensor was ±0.4% of the full range, and the pressure ranges were 0~25 bar and 0~40 bar, respectively.

For the measurement of the water, 2 PT1000 temperature sensors were attached to the supply and return pipes of the unit to acquire the changes of the supply and return water temperature. The accuracy and range were the same as that used in the ASHP unit measurement. In addition, an electromagnetic flowmeter was also installed at the supply water pipe of the unit to monitor the changes of flow rates of the circulating water. The accuracy of the flowmeter was ±0.5% of full range, and the measuring range was 0.5~10 m^3/h.

Additionally, a digital camera with a resolution of 150 pix was installed near the outdoor heat exchanger to record the real-time frosting process on the fins. Three heating power sensors were also used in the measurement to acquire the power input of the ASHP units and the circulating water pumps.

Finally, in terms of the frosting map that was presented by Wang et al. [21], 3 typical frosting conditions were selected in the field measurement to scrutinize the frosting behaviors of the ultra-low temperature ASHP units. The details are given in Figure 2. Among these 3 typical frosting conditions, case 1, case 2, and case 3 of this study correspond to the severe frosting region, moderate frosting region, and mild frosting region, respectively. Moreover, the reverse-cycle defrosting method was used in the tested ASHP unit. For reverse-cycle defrosting, the outdoor heat exchanger changed from evaporator to condenser, while the indoor heat exchanger became the evaporator, and the energy originally used to heat a room would be used to heat the outdoor exchanger [22]. Furthermore, a conventional defrosting initiation method, the Temperature-Time (T-T) method [1,21], was used to initiate defrosting of the two field ASHP.

2.3. Data Analysis

In this study, the *COP* was selected as a critical indictor for the frosting-suppression and heating performance of the ASHP unit, as usually used in similar studies. Moreover, the frosting time, the suction and discharge pressures, and the temperature of the coils were also recorded and analyzed. The *COP* indicates the heating capacity of the ASHP unit by consuming a certain amount of electric power, it can be calculated using Equations (1) and (2).

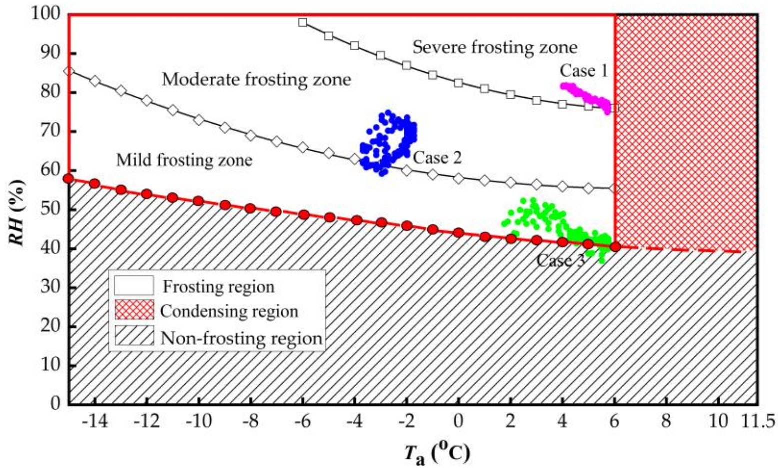

Figure 2. Typical frosting condition in the frosting map developed by Wang et al. [21].

$$COP = \frac{\int_0^{t_n} q\mathrm{dt}}{\int_0^{t_n} W\mathrm{dt}} \tag{1}$$

$$COP_{\mathrm{sys}} = \frac{\int_0^{t_n} q\mathrm{dt}}{\int_0^{t_n} (W+P)\mathrm{dt}} \tag{2}$$

In the above formulas, q was the instant heating capacity of the unit and could be calculated using $q = \mathrm{m_w c_p \Delta T_w}$. Where $\mathrm{m_w}$ was the flow rate of the water, $\mathrm{c_p}$ was the specific heat at constant pressure, and $\Delta \mathrm{T_w}$ was the temperature differences between the supply and return water. W represented the power of the units, P represented the power input of the water pump, and t_n denoted the defrosting time of the unit.

In addition, the equivalent energy consumption Q_s, the annual cost AC, as well as the payback period of the additional investment t_hs were selected as the economic and environmental criteria of the unit. These indexes can be calculated using Equations (3)–(6).

$$Q_\mathrm{s} = \frac{Q_\mathrm{h}}{\eta_\mathrm{t} \times q} - \frac{D \times Q_\mathrm{h}}{3.6 \times COP_{\mathrm{sys}}} \tag{3}$$

$$AC = C_o + C_m + (A/P, i, j)(C - B) + Bi \tag{4}$$

$$(A/P, i, j) = \frac{i}{1 - (1+i)^{-j}} \tag{5}$$

$$t_\mathrm{hs} = \frac{\Delta C}{\Delta C_o} \tag{6}$$

In the calculation of the Q_s, q represented the calorific value of the standard coal (29.307 MJ/kgce), and Q_h was the total heating capacity of the unit, η_t denoted the thermal efficiency when using the conventional energy source, and the value was 0.7 when using the coal as the heating source [23]. D was power input corresponding to the standard coal, and it was 0.3 kgce/kWh in terms of the latest data published by National Bureau of Statistics in China [24]. COP_{sys} represented the heating performance efficient of the heat pump system. C_o was the annual operation cost of the unit. C_m meant the annual maintenance cost, which was usually regarded as 6% of the total cost of equipment [24]. (A/P,i,j) was the coefficient of the payback. C was the total initial investment of the ASHP unit, B meant the net salvage value of the ASHP unit. i denoted the constant discount rate of the unit, which was set as 4.594%, according to a previous study [25]. j represented the whole life circle of the unit, ΔC was the additional investment, and ΔC_o represented the annually saved cost.

Finally, the relative uncertainty analysis was used in the data analysis, considering that the errors due to the direct measurement would inevitably transfer to the indirect measured data and thus produce indirect measurement errors [26]. The relative uncertainty U_r was selected in this study to eliminate the indirect errors. The related calculation was given as Equations (7)–(9).

$$N = f(X, Y, Z \ldots) \tag{7}$$

$$\delta_{\overline{N}} = \sqrt{\left(\frac{\partial f}{\partial X}\delta_{\overline{X}}\right)^2 + \left(\frac{\partial f}{\partial Y}\delta_{\overline{Y}}\right)^2 + \left(\frac{\partial f}{\partial Z}\delta_{\overline{Z}}\right)^2 + \cdots} \tag{8}$$

$$U_r = \frac{\delta_{\overline{N}}}{\overline{N}} \tag{9}$$

where N represented the indirect measured parameter, such as COP and instant heating capacity. X, Y, and Z were the related parameters that were used to calculate N. $\delta_{\overline{N}}$ meant the standard uncertainty.

3. Results and Discussions

3.1. Environmental Data during the Measurement and the Predicted Frosting Levels

The outdoor environmental conditions during the 38-day field measurements were recorded and analyzed. Results were depicted in Figure 3. The daily air temperature ranged between −1.85 °C and 15 °C, and the daily relative humidity ranged between 24.4% and 81.3%. The daily outdoor air temperature and relative humidity were negatively correlated. The mean daily outdoor air temperature and relative humidity were 5.7 °C and 45.8%, respectively.

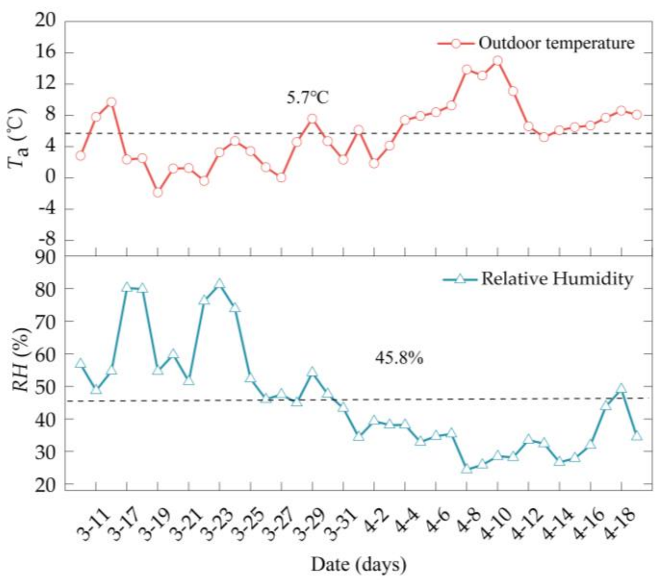

Figure 3. Changes of the daily outdoor temperature and relative humidity during the field measurements.

Based on the outdoor temperature and relative humidity during the field measurements and the frosting map developed by Wang et al. [21], the frosting levels during the whole field measurement were predicted, and the results are shown in Figure 4. The severe frosting condition accounted for 7.8% of the whole operation time of the ASHP unit, while the moderate frosting and mild frosting accounted for 13.1% and 19.3%, respectively. The total frosting period could reach up to 40.3% of the whole 38 days. Additionally, as can be seen in Figure 4, the hourly minimum value of the outdoor ambient temperature reached −7 °C.

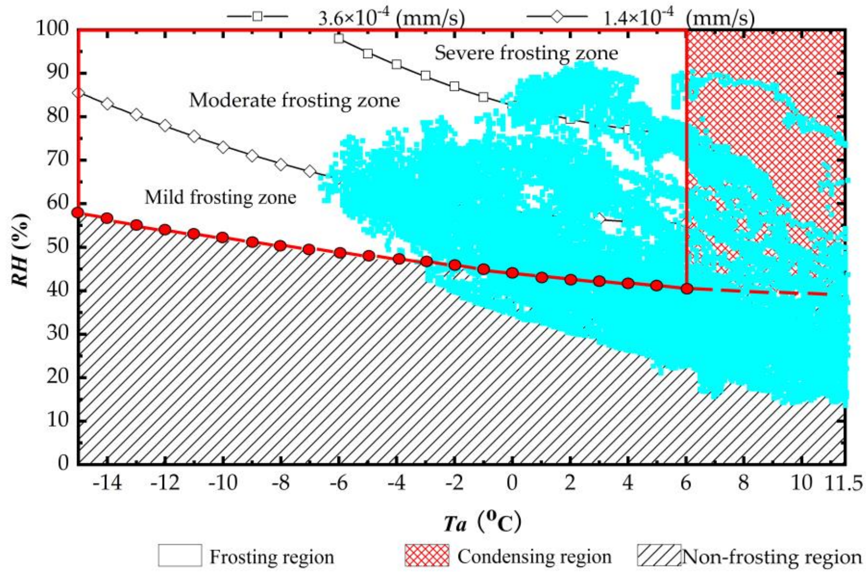

Figure 4. Distribution of the frosting levels during the whole field measurement.

3.2. Actual Performance of the New ASHP Units under Three Typical Frosting Conditions

Based on the predicted frosting levels of the three cases, it was necessary to observe the actual frosting levels when the ultra-low temperature ASHP units was used during the field measurement. The images of the frosting levels on the outdoor heat exchanger fins before the ASHP unit started to defrost are given in Table 3, as well as shown the recorded frosting time. The results indicated that only moderate frosting was observed on the outdoor fins of the ultra-low temperature ASHP units in case 1, under the severe frosting condition as predicted by the frosting map. Specifically, the frosting only occurred on the upper parts and the bottom of the outdoor heat exchangers, the frost did not cover all the fin surface. However, in case 2, predicted as the moderate frosting condition, only mild frosting was observed, and no frost was spotted in case 3, regarded as the mild frosting condition. These images suggested that the frosting of the ultra-low temperature ASHP units was greatly attenuated compared with the traditional ASHP unit.

Table 3. The actual frosting levels and the recorded frosting time of the new ASHP.

Frosting Condition	Case 1	Case 2	Case 3
The actual frosting levels	 Moderate frosting	 Mild frosting	 Zero frosting
The actual frosting time	109 min	114 min	/
Frosting predicted by Reference [21]	$t \leq 30$ min Severe frosting	30 min $\leq t \leq$ 90 min Moderate frosting	90 min $\leq t \leq$ 150 Mild frosting

Moreover, the frosting time recorded by the camera for these three cases was 109 min, 114 min, and 0 min (no frost), respectively. The frosting time of the new ASHP units was longer than that predicted by Reference [21], which produced strong evidence for the enhanced frosting-suppression capability of the ultra-low temperature ASHP unit.

Furthermore, the heating performance of the new ASHP units were also scrutinized based on the measured data. The results are given in Figure 5. The outdoor air temperature and relative humidity were stable for all three cases. In case 1, the coil temperature of the outdoor heat exchanger of the new ASHP units was reduced, due to the effect of moderate frosting on the fin. The lowest coil temperature was found at −18.4 °C. Consequently, the heating capacity and the *COP* of the new ASHP units was reduced by 35.5% and 30.3% in case 1, respectively.

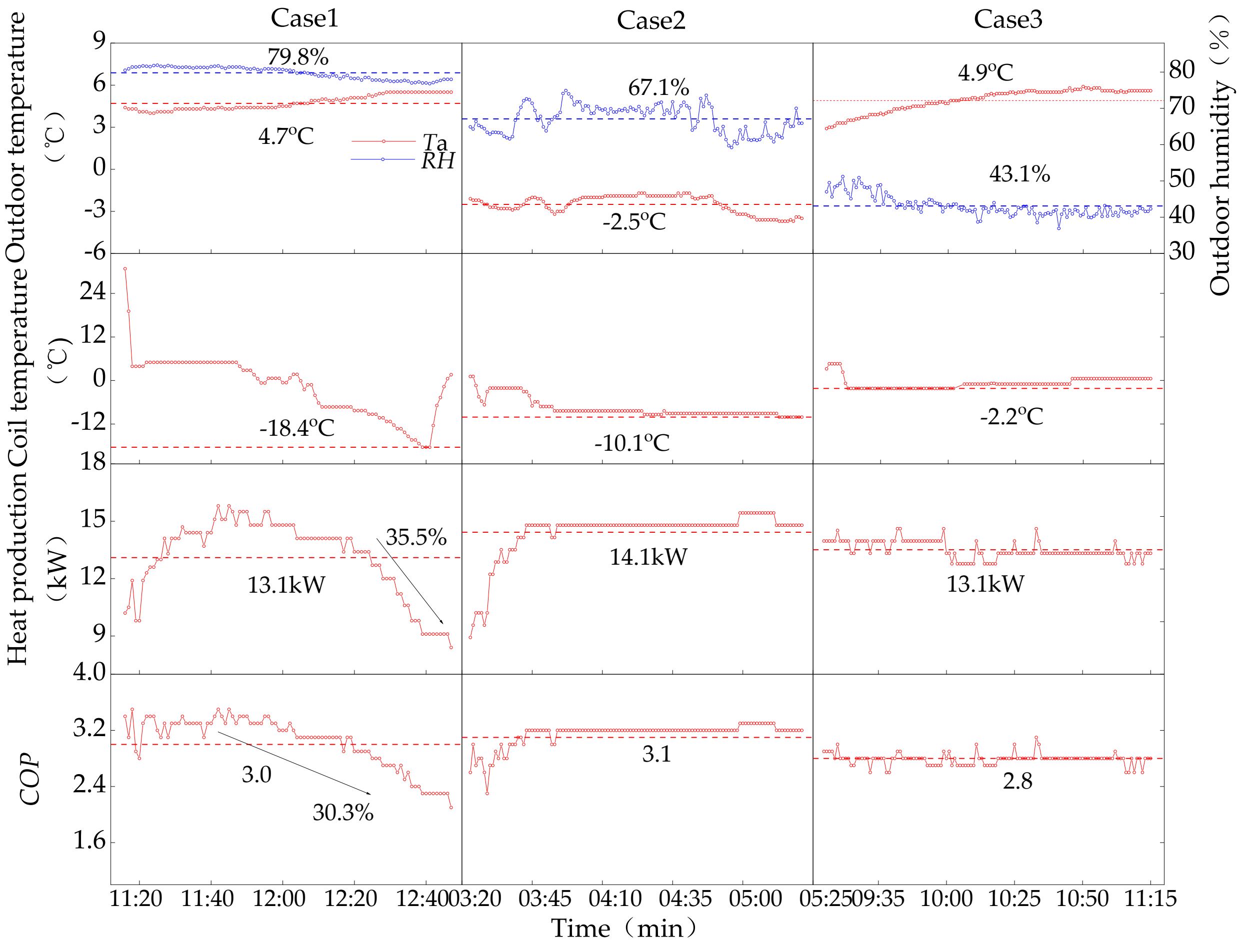

Figure 5. Heating performance of the ASHP under typical frosting conditions.

However, both the heating capacity and the *COP* of the unit in case 2 and case 3 were found to be much more stable than case 1. The heating capacity and *COP* of case 2 were 14.1 kW and 3.1, respectively, while for case 3, they were 13.1 kW and 2.8, respectively. The results suggested that both case 2 and case 3 were less affected by the frosting. These findings were in accordance with the results in Table 3. Specifically, the moderate frosting attenuated the performance of the ASHP unit, while the mild frosting and zero frosting had less negative contribution to the performance of the unit. Furthermore, Table 4 shows the relative uncertainty values of *COP* for the measured unit in the three cases. The relative uncertainty values of *COP* in the three field measurement cases ranged from 3.6% to 4.3%, suggesting an acceptable measuring accuracy.

Table 4. The relative uncertainty values of *COP* for the test unit in the three field test cases.

Parameter	Case 1	Case 2	Case 3
$U_r(COP)$	4.3	3.7	3.6

3.3. Long-Term Performance of the New ASHP in Regular Heating Season

In order to investigate the long-term performance of the ultra-low temperature ASHP unit, all these indexes used in field measurements were also recorded during the regular heating season of the office building. The results are shown in Figure 6, including the indoor air temperature T_n, the heating capacity per square meter q_0, the temperature differences between the supply and return water ΔT, and the COP.

As depicted in Figure 6a, the mean indoor air temperature during the heating season reached up to 24.56 °C. And the mean temperature difference between the supply and return water was 4.18 °C, which suggested that the load rate reduced gradually as the outdoor air temperature increased, but the temperature differences between the supply and return water stayed stable, leading to a higher indoor air temperature of up to 28 °C in the last part of the whole measurement. In addition, it was found that the heating capacity per square meter q_0 reached 21.34 W/m^2, and the mean COP was 3.34 during the whole measurement, which implied the improved continuous heating performance and frosting-suppression capability under cold environmental conditions.

Figure 6b describes the system performance of the ASHP unit. Changes of the indices, such as the heating capacity per square meter of the system (q_{sys}), the heating performance efficient of the heat pump system (COP_{sys}), and the power input of the water pump (P), were analyzed. During the heating season, the mean q_{sys} reached up to 20.97 W/m^2, the mean COP_{sys} was 2.63, and the mean power input of the water pump was 1.0 kW. As shown in Table 5, by conducting the relative uncertainty analysis, the relative uncertainty of the calculated q_0, COP, q_{sys}, and COP_{sys} were 3.7%, 4.3%, 3.8%, and 4.6%, respectively. These small uncertainty values revealed that the indirect errors were greatly eliminated, and the results calculated were reliable.

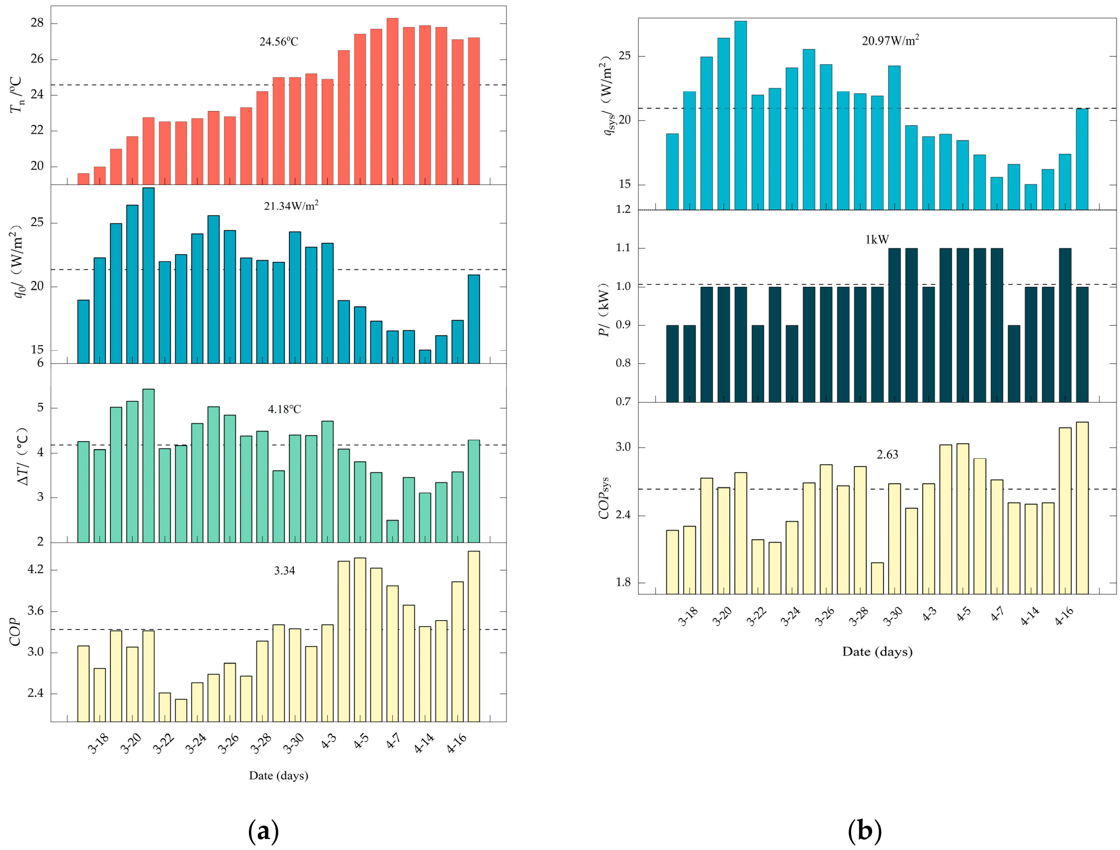

Figure 6. Performances of the new ASHP unit and system during long term operation. (**a**) Performances of the new ASHP unit during long term operation. (**b**) Performances of the new ASHP system during long term operation.

Table 5. The relative uncertainty values of *COP* for both units in the three field test cases.

Parameter	$U_r(q_0)$	$U_r(COP)$	$U_r(q_{sys})$	$U_r(COP_{sys})$
Values	3.7%	4.3%	3.8%	4.6%

3.4. Environmental and Economic Benefits of the ASHP

3.4.1. Environmental Benefits Analysis

According to the long-term field measurement in the heating season, the total heating load was 174,821.8 MJ per year. In terms of the calculation of the equivalent energy consumption Q_s, the Q_s of the ultra-low temperature ASHP unit in the heating season was 2961.2 kgce.

Based on the calculated Q_s, the annual CO_2 emission reduction in the ASHP unit was also calculated through the standard coal coefficient method recommended by GB/T 50801-2013. Results showed that the carbon emission reduction in the ASHP was 7314.2 kg per year. Considering the heating area of the office building in this study, the carbon emission reduction in the new ASHP unit was 11.3 kg per year per square meter, which produced great environmental benefits compared with the traditional central heating system through the coal-fired boilers in thermal power plants.

3.4.2. Economic Benefits Analysis

The economic benefits were analyzed in terms of the total annual cost (*AC*), and the payback period of the additional investment (t_{hs}) on the ASHP unit. Less annual cost corresponds to the better choice.

According to the local power price 0.47 Yuan/kWh that was provided by the local government, and the mean *COP* of the ASHP (2.1) recommended by a report published by Chinese Academy of Building Science [27], the annual costs of operation of the conventional and the ultra-low temperature ASHP were 10,901 Yuan and 8687 Yuan, respectively. In addition, the initial investment C and net salvage B of the conventional ASHP unit were 6800 Yuan and 680 Yuan, respectively, while for the new ASHP unit, they were 9000 and 900 Yuan, respectively. Furthermore, as recommended by Reference [24], the annual cost of maintenance was 6% of the initial investment. Therefore, the cost on maintenance was 408 Yuan for the conventional ASHP, and 540 Yuan for the new ultra-low temperature ASHP unit.

Therefore, the total annual costs (*AC*) of the convectional and new ASHP unit were 11,914 and 10,027 Yuan, respectively. The detailed results were given in Table 6. The results suggested that the total annual cost of the ultra-low temperature ASHP unit was 1887 Yuan less than that of the conventional ASHP unit, corresponding to a cost reduction of 15.8%.

Table 6. Comparison of the total annual cost of the conventional and ultra-low temperature ASHP.

	C (Initial Investment)/CNY	B (Net Salvage)/CNY	Co (Annual Cost on Operation)/CNY	Cm (Annual Cost on Maintenance)/CNY	AC (Annual Cost)/CNY
Conventional ASHP	6800	680	10,901	408	11,914
Ultra-low temperature ASHP	9000	900	8687	540	10,027

The payback period of the additional investment (t_{hs}) on the ASHP unit is another important economic index. In order to realize the performance under cold environment, Additional investment was required to add on critical components, including the outdoor heat exchanger, the outdoor fan and the sheet metal processing. The detailed comparison of the cost on critical components between the conventional and ultra-low temperature ASHP unit was provided in Table 7.

As indicated in Table 7, the additional investment on the ultra-low temperature ASHP was 1827 Yuan. However, the total annual cost of the ultra-low temperature ASHP unit was 1887 Yuan, which was less than the conventional unit. According to the calculation of the payback period of the additional investment (t_{hs}), the payback time of the ultra-low temperature ASHP was 0.97 year.

Table 7. Cost on the components of the conventional and ultra-low temperature ASHP.

Component	Conventional ASHP (CNY)	Ultra-Low Temperature ASHP (CNY)	Difference (CNY)
Compressor	900	1200	300
Outdoor heat exchanger	850	1430	580
Outdoor fan	60	220	160
Sheet metal processing	550	1337	787
Total	2360	4187	1827

4. Conclusions

Field measurement and long-term operation of the ultra-low temperature ASHP were carried out in this study to scrutinize the performance of the ASHP unit in cold regions. The main findings were obtained and presented below.

(1) In an experimental psychrometric chamber environment, the *COP* of the ultra-low temperature ASHP reached up to 1.83 at the extremely low outdoor air temperature of −25 °C with a heating power of 7.5 kW.

(2) Improved defrosting capabilities of the ultra-low temperature ASHP were observed through the field measurement under three typical frosting conditions. The heating capacity and the *COP* of the unit in case 2 and case 3 were found to be much more stable than that of case 1, suggesting that both case 2 and case 3 were less affected by the frosting. Specifically, only moderate frosting was detected under the severe frosting condition, and mild frosting was observed under the moderate frosting condition. Under the mild frosting condition, however, no frosting occurred.

(3) The heating performance of the ultra-low temperature ASHP in long-term operation was investigated, which achieved a mean *COP* of 3.34, a mean COP_{sys} of 2.63, and a mean heating capacity of 21.34 W/m^2 during the heating season. The results suggested that the improvement of continuous heating performance and frosting-suppression capability under cold environmental conditions was achieved.

(4) Better environmental and economic benefits were observed. Specifically, the ultra-low temperature ASHP had a carbon reduction of 11.3 kg per year per square meter, while its total annual cost was 1887 Yuan, 15.8% less than that of the conventional ASHP unit. The payback period of the additional investment was only 0.97 years. The results showed that the ultra-low temperature ASHP unit had better environmental benefits and economic benefits.

Author Contributions: Methodology, Y.D.; Investigation, X.L. (Xueli Lian), X.L. (Xiaolong Li) and D.B.; Resources, J.L.; Writing—original draft, C.Z.; Writing—review & editing, C.Z.; Project administration, Y.D.; Funding acquisition, Y.D. All authors have read and agreed to the published version of the manuscript.

Funding: The project (2021EEDSCXQDFZ009) is supported by the Ordos Science and Technology Plan.

Acknowledgments: The project (2021EEDSCXQDFZ009) is supported by the Ordos Science and Technology Plan. Thank you to Hui Zhu of the Qingdao University of Technology for his careful editing service.

Conflicts of Interest: The authors declare no conflict of interest.

References

1. Chen, X.; Hao, B.; Liu, S.; Zhou, W.; Yao, C.; Wang, S. Study on Demand-side Design Parameters of Solar Domestic Hot Water System in Residential Buildings. *Energy Procedia* **2015**, *70*, 340–346. [CrossRef]
2. Sun, X.; Yao, C.; Zhao, H.; Dai, Y. Research on roadmap of taking air thermal energy into the scope of renewable energy sources. *Chin. J. Refrig. Technol.* **2015**, *35*, 36–40.
3. Hou, L.; Ding, H.; Liu, Y.; Wang, S. Evaluation and suggestion on the subsidy policies for rural clean heating in winter in the Bei-jing-Tianjin-Hebei region. *Energy Build.* **2022**, *274*, 112456. [CrossRef]
4. Ma, L.; Liu, Z.; Zhang, X.; Zhang, C. Design and thermodynamic optimization of enhanced Vapor injection technology in double stage coupling heat pump. *Build. Energy Environ.* **2016**, *35*, 17–21.
5. Chen, J.; Yang, C.; Cai, B. Experimental of low temperature heat flash type air source heat pump water heater. *Fluid Mach.* **2010**, *38*, 72–74.
6. Wu, C.; Liu, F.; Li, X.; Wang, Z.; Xu, Z.; Zhao, W.; Yang, Y.; Wu, P.; Xu, C.; Wang, Y. Low-temperature air source heat pump system for heating in severely cold area: Long-term applicability evaluation. *Build. Environ.* **2022**, *208*, 108594. [CrossRef]
7. Safa, A.A.; Fung, A.S.; Kumar, R. Comparative thermal performances of a ground source heat pump and a variable capacity air source heat pump systems for sustainable houses. *Appl. Therm. Eng.* **2015**, *81*, 279–287. [CrossRef]
8. Zhang, Y.; Ma, Q.; Li, B.; Fan, X.; Fu, Z. Application of an air source heat pump (ASHP) for heating in Harbin, the coldest provincial capital of China. *Energ. Build.* **2017**, *138*, 96–103. [CrossRef]
9. Zhang, H.; Jiang, L.; Zheng, W.; You, S.; Jiang, T.; Shao, S.; Zhu, X. Experimental study on a novel thermal storage refrigerant-heated radiator coupled with air source heat pump heating system. *Build. Environ.* **2019**, *164*, 106341. [CrossRef]
10. Standardization Administration of China. *GB/T25127.1*; Low Ambient Temperature Air Source Heat Pump (Water Chilling) Packages—Part 1: Heat Pump (Water Chilling) Packages for Industrial & Commercial and Similar Application. Standards Press of China: Beijing, China, 2020.
11. Standardization Administration of China. *GB/T25127.2*; Low Ambient Temperature Air Source Heat Pump (Water Chilling) Packages—Part 2: Heat Pump (Water Chilling) Packages for House Hold and Similar Application. Standards Press of China: Beijing, China, 2020.
12. Liang, S.; Wang, H.; Gao, X.; Tian, X.; Zhu, H.; Hu, S.; Lin, C. Experimental study on the operating performance of the air source heat pump (ASHP) with variable outdoor airflow rate under the standard frosting condition. *Energy Built Environ.* **2023**. [CrossRef]
13. Dong, J.; Deng, S.; Jiang, Y.; Xia, L.; Yao, Y. An experimental study on defrosting heat supplies and energy consumptions during a reverse cycle defrost operation for an air source heat pump. *Appl. Therm. Eng.* **2012**, *37*, 380–387. [CrossRef]
14. Liu, J.; Sun, Y.; Wang, W.; Zhu, J. Performance evaluation of air source heat pump under unnecessary defrosting phenomena for nine typical cities in China. *Int. J. Refrig.* **2016**, *74*, 385–398. [CrossRef]
15. Qu, M.; Xia, L.; Deng, S.; Jiang, Y. An experimental investigation on reverse-cycle defrosting performance for an air source heat pump using an electronic expansion valve. *Appl. Energy* **2012**, *97*, 327–333. [CrossRef]
16. Wu, Y.; Wang, W.; Sun, Y.; Cui, Y.; Lin, Y. Development of evaluation indexes for assessing the regional operating performances of air source heat pump (ASHP) units operated in different climate regions based on the equivalent temperature drop method. *Energy Build.* **2021**, *247*, 111111. [CrossRef]
17. Wang, W.; Guo, Q.C.; Feng, Y.C.; Lu, W.P.; Dong, X.G.; Zhu, J.H. Theoretical study on the critical heat and mass transfer characteristics of a frosting tube. *Appl. Therm. Eng.* **2013**, *54*, 160. [CrossRef]
18. Wang, W.; Feng, Y.C.; Zhu, J.H.; Li, L.T.; Guo, Q.C.; Lu, W.P. Performances of air source heat pump system for a kind of mal-defrost phenomenon appearing in moderate climate conditions. *Appl. Energy* **2013**, *112*, 1138–1145. [CrossRef]
19. Guo, X.M.; Chen, Y.G.; Wang, W.H.; Chen, C.Z. Experimental study on frost growth and dynamic performance of air source heat pump system. *Appl. Therm. Eng.* **2008**, *28*, 2267–2278. [CrossRef]
20. Wang, W.; Xiao, J.; Guo, Q.C.; Lu, W.P.; Feng, Y.C. Field test investigation of the characteristics for the air source heat pump under two typical mal-defrost phenomena. *Appl. Energy* **2011**, *88*, 4470–4480. [CrossRef]
21. Zhu, J.H.; Sun, Y.Y.; Wang, W.; Deng, S.M.; Ge, Y.J.; Li, L.T. Developing a new frosting map to guide defrosting control for air-source heat pump units. *Appl. Therm. Eng.* **2015**, *90*, 782–791. [CrossRef]
22. Wu, C.; Wang, Z.; Li, X.; Xu, Z.; Xu, C.; Yang, Y.; Zhao, W.; Wang, Y. Field experimental research on retarding frosting and improving defrosting performance of air source heat pumps through variable frequency technology. *J. Build. Eng.* **2023**, *64*, 105628. [CrossRef]
23. China Association for Engineering Construction Standardization. *T/CECS 564-2018*; Technical Specification for Air Source Heat Pump Heating System. Architecture & Building Press: Beijing, China, 2018.
24. Yang, H. Annual-cost Analysis and Application of Ground-Water Heat Pump System. Bachelor's Thesis, Tianjin University, Tianjin, China, 2005.
25. Steiner, H.M. *Engineering Economic Principles*; Economic Science Press: Beijing, China, 2000.

26. Bai, X.; Wang, W.; Sun, Y.; Liu, J.; Ge, Y.; Deng, S. Operating performances of an ASHP unit operated in a mild and humid region using tube-encircled photoelectric sensor based defrosting initiation strategy. *Energy Build.* **2018**, *177*, 140–153. [CrossRef]
27. Xu, Z.; Zhao, W.; Shao, S.; Wang, Z.; Xu, W.; Li, H.; Wang, Y.; Wang, W.; Yang, Q.; Xu, C. Analysis on key influence factors of air source heat pumps with field monitored data in Beijing. *Sustain. Energy Technol. Assess.* **2021**, *48*, 101642. [CrossRef]